VOLUME 3, NUMBER 8, AUGUST 2003

NANO LETTERS

Simulated Assembly of Nanostructured Organic/Inorganic Networks

Monica H. Lamm,[†] Ting Chen,[†] and Sharon C. Glotzer*[,†,‡]

Departments of Chemical Engineering and Materials Science and Engineering, University of Michigan, Ann Arbor, Michigan 48109-2136

Received February 17, 2003; Revised Manuscript Received March 25, 2003

ABSTRACT

We perform lattice Monte Carlo simulations to study nanostructured networks formed by linking organically functionalized inorganic nanoscale building blocks. We develop a minimal lattice model of an octafunctional nanoscale building block (NBB) by representing the inorganic core with a rigid cube and the organic linkers with "bead-spring" chains. Using this model, we explore the effect of linker length on network properties including porosity, spatial distribution of NBBs, and extent of cross-linking during assembly. We compare our results with recent experimental data on networks of octafunctional polyhedral oligomeric silsesquioxane (POSS) cubes.

An impressive variety of nanoparticles and supramolecular structures with nanoscale dimensions such as nanorods,[1,2] nanocubes,[3] nanoprisms,[4,5] nanotubes,[6,7] fullerenes,[8−10] cubic silsesquioxanes,[11−17] and quantum dots[18,19] are available today. The functionalization of these nanoscale "building blocks" (NBBs) opens exciting new avenues for creating designer materials and devices by directed assembly. In particular, advances in synthetic chemistry have made it possible to attach either synthetic or biological macromolecules to the NBBs. Highly specific "lock-and-key" recognitive interactions among these organic groups can then be utilized as a means of coaxing the NBBs into ordered one-, two-, and three-dimensional structures. There are several experimental "proof-of-concept" examples[20−25] demonstrating that suitably functionalized NBBs can be assembled into rather simple structures. Although some of the nanostructures attained in this way suggest the possibility of tremendous technological potential, the full realm of diversity in the structure and functionality of nanoscale architectures has yet to be realized. In fact, very little of the vast parameter space of these complex assemblies has been explored to date. Computer simulations and theory can help identify and efficiently map the parameter space as well as provide fundamental insight into the directed assembly process. By combining insights gained from theory, experiment, and simulation, it should be possible to construct a rational approach to the design of novel and useful nanostructures obtained via directed assembly of functionalized NBBs.

Here, we present Monte Carlo simulations of nanostructured networks formed by cross-linking model functionalized NBBs. We compare our results to experiments performed on organic/inorganic hybrid polyhedral oligomeric silsesquioxane (POSS) networks[13,26] to illustrate how our simulation approach provides insight. Although we focus the discussion on a specific system, we expect these results and our computational strategy to be applicable in the broader context of nanoscale assembly.

* Corresponding author. E-mail: sglotzer@umich.edu.
[†] Department of Chemical Engineering.
[‡] Department of Materials Science and Engineering.

10.1021/nl034090s CCC: $25.00
Published on Web 04/30/2003

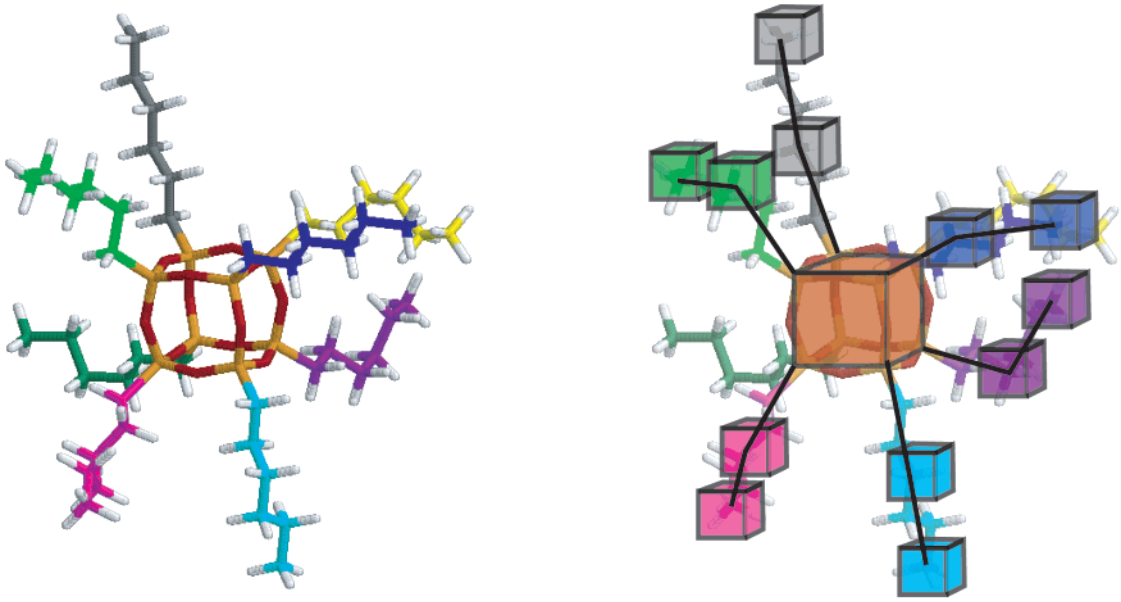

Figure 1. Our coarse-grained model for functionalized cubic NBBs mapped to octa(hexyl)-POSS $[CH_3(CH_2)_5SiO_{1.5}]_8$. The stick model on the left shows the POSS cage composed of Si (orange) and O (red) atoms and the organic linkers, where the backbone atoms of each linker are drawn with different to colors to distinguish the otherwise identical linkers. The schematic on the right shows the coarse-grained model (cubes) superimposed on the atomistic model. For clarity, only selected linkers are "coarsened" in this schematic.

The computational challenge of simulating large collections of functionalized NBBs assembling into larger-scale structures can be alleviated to some degree by restricting the motion of NBBs and linkers to the vertices of a finely grained lattice. The assembly of functionalized NBBs in this study is simulated using lattice Monte Carlo with the bond fluctuation (BF) model and algorithm.[27−29] The BF lattice algorithm has been widely adopted for the simulation of polymer network formation.[30−37] In the present application of the BF model, the fundamental building block of the network is composed of a NBB with eight chainlike functional groups of equal length. We model the NBB as a rigid cube occupying $3 \times 3 \times 3$ lattice vertices. Attached to each corner of the rigid cube is a flexible, short-chain linker. Each linker consists of L connected monomers, where each monomer occupies $2 \times 2 \times 2$ lattice vertices. In this work, we consider NBBs functionalized with linkers containing $L = 1$, 2, 3, and 4 monomers. Following the original implementation of the bond fluctuation model, the allowed bond vectors between two consecutive linker segments are the following: [2, 0, 0], [2, 1, 0], [2, 1, 1], [2, 2, 1], [3, 0, 0], and [3, 1, 0]. To facilitate the diffusion of the rigid NBB core (and thus the entire octafunctional unit), the set of allowed bond vectors between a linker segment and a NBB includes the bond vectors listed above and these additional vectors: [3, 1, 1], [3, 2, 1], [4, 0, 0], and [2, 2, 2].[38]

The model described above is considered to be a coarse-grained model because each NBB or linker segment is intended to mimic the conformational and space-filling characteristics of a collection of atoms rather than represent the atomistic details explicitly. Despite this seemingly drastic simplification, our model may be mapped onto a specific system. For example, we map our coarse-grained NBB/linker model to a functionalized POSS $[RSiO_{1.5}]_8$ molecule. This POSS molecule has a well-defined cubic cage with Si atoms at the corners and O atoms along the edges; the functional group R can be reactive (a linker) or nonreactive and is attached at the Si corners. The flexibility of the Si_8O_{12} cage depends on the functional group R. Principal component analysis[39] on the crystal structures of $H_8Si_8O_{12}$, $(CH_3)_8Si_8O_{12}$, and $(C_2H_5)_8Si_8)O_{12}$ have shown deformations in the Si_8O_{12} cage structure of 14, 3, and 1%, respectively. Since the present work considers only the case of R = alkyl, the Si_8O_{12} cage is modeled as a rigid cube. The representation of the Si_8O_{12} cage as a rigid object in this model is further justified by noting that ~10 GPa of hydrostatic tensile stress is required to cause a 1% deformation along the Si−O−Si bonds (vibrational frequency[40] ≈ 1000 cm^{-1}) of the cage. The cage dimensions are ~0.54 nm along the body diagonal between Si atoms and ~0.32 nm along the edge between Si atoms. Using these dimensions of the Si_8O_{12} cage as a basis for a "rigid" cube, one lattice spacing in our model corresponds to 0.16 nm. Next, we must gauge how many groups of atoms are represented by a linker segment. As a rough estimate,[41] we computed the radius of gyration and corner-to-end distance (Si atom to last backbone atom on linker) of the linkers for atomistic models of a series of alkyl-POSS[42] and compared them to those obtained for the coarse-grained NBB/linker model with $L = 1$, 2, 3, and 4. We find that one linker segment maps to approximately three CH_2 groups. Figure 1 shows an example of the coarse-grained model for an octafunctional NBB with linkers of length $L = 2$ mapped to an atomistic model of octa(hexyl)-POSS. We emphasize that the model NBB could be constructed to represent any nanoparticle or supramolecular object geometrically by selecting an appropriate size, shape, aspect ratio, functionality, and arrangement of functional groups on the surface.

The networks are prepared in the following manner. Prior to the simulation, $N = 4500$ octafunctional NBBs are

randomly placed on a cubic lattice at a volume fraction of $\phi = 0.05$. This volume fraction corresponds to octafunctional NBB concentrations ranging from 0.13 g/mL ($L = 1$) to 0.17 g/mL ($L = 4$) when our coarse-grain mapping for alkyl-POSS is applied to the model. The total number of linker segment and NBB "movable units" ranges from 40 500 in the $L = 1$ system to 148 500 in the $L = 4$ system. The system is relaxed athermally (i.e., only excluded volume interactions and the connectivity among the linker segments and NBBs are considered) for $(6-10) \times 10^5$ Monte Carlo steps, where a Monte Carlo step consists of $8LN$ attempted monomer displacements and N attempted rigid cube displacements. The linker segments and NBB of the octafunctional unit move in the following manner. A linker segment or NBB is selected at random and displaced one lattice unit in a randomly chosen direction. The displacement move is accepted if the neighboring sites in the direction of the move are unoccupied and if the resulting bond vector(s) is in the set of allowed bond vectors. The system is deemed to be sufficiently relaxed when the octafunctional units have, on average, undergone a net displacement a distance greater than their radius of gyration.[43] For the $L = 4$ system, this typically requires as many as 1×10^6 Monte Carlo steps or 95 CPU hours on a single AMD Athlon MP processor running at 1.4 GHz.

Once the configuration has relaxed, cross-linking interactions are introduced between nearest-neighbor (distance vector [2, 0, 0]) linker ends to form tethers between the NBBs. The energy of interaction between nearest-neighbor linker ends is $\epsilon/k_BT = -10$, where ϵ is the cross-link bond energy, k_B is the Boltzmann constant, and T is the system temperature. The value of ϵ/kT was chosen to give a low probability of cross-link breakage. The cross-linking was stopped after some time t_{cure} (in MC steps) when the fraction of unreacted linkers reached a steady-state value.

Figure 2 contains snapshots of the networks made by cross-linking NBBs functionalized with linkers $L = 1$, 2, and 4. Qualitatively, one can observe that the degree of porosity in the networks decreases as the linker length increases by the presence of large voids in the small-L networks and the absence of large voids in the large-L networks.

To measure the spatial distribution of NBBs in the assembled networks, we compute the static structure factor, $S(k)$, of the tethered NBBs by calculating the Fourier transform of the NBB pair-correlation function. Figure 3 shows the structure factor $S(k)$ as a function of scattering vector k obtained for the four networks. Moving from values of high to low k, the structure factor goes through a peak at intermediate k followed by a steep upturn at low k. The peak at intermediate k corresponds to the average distance between NBBs through the relation $r_{av} = 2\pi/k$. As the linker length increases, this peak appears at larger distances (lower k), demonstrating an increased average spacing between NBBs for larger L. The steep upturn at low k indicates a periodicity in the network structure at a correlation length larger than the size of our simulation box.

To determine whether the resulting structure is a single network of NBBs spanning the simulation cell or a collection of smaller aggregates, we use an analysis algorithm developed in our group called TINGFO,[44] modeled after the SPANFO[45] algorithm for determining connectivity in graphs. It can be used for both lattice and continuum systems to calculate the number of network structures in a system and the number of network defects such as soluble material, dangling ends, loops, and large pendent structures. Using TINGFO, we find that all of the assembled networks are single, cell-spanning networks composed of nearly all (>99%) the NBBs in the system. However, whereas the number of NBBs in the network remains constant, the fraction of unreacted linkers increases as L increases. Additionally, the elastically active fraction of network material (all NBBs and linkers minus network defects)

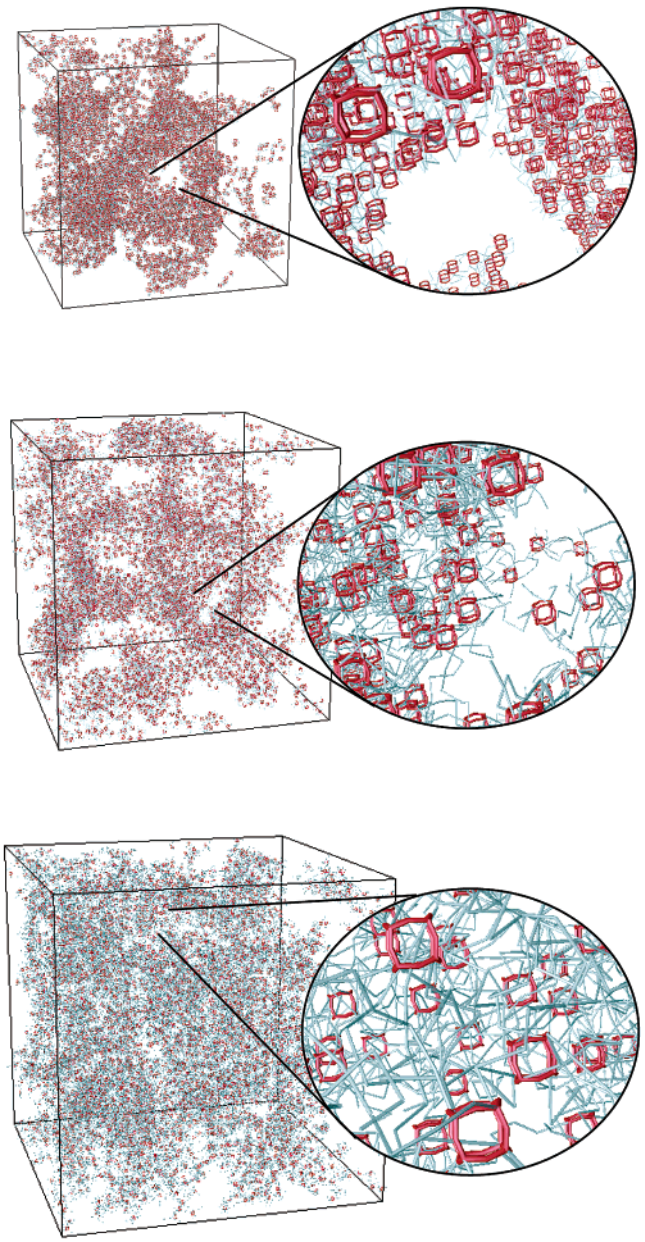

Figure 2. Snapshots of the organic/inorganic networks simulated using lattice Monte Carlo and the bond fluctuation model with (top to bottom) L equal to 1, 2, and 4. The red cages are the inorganic silsesquioxanes, and the gray sticks are the organic linkers. All systems shown contain 4500 functionalized NBBs at a volume fraction of $\phi = 0.05$.

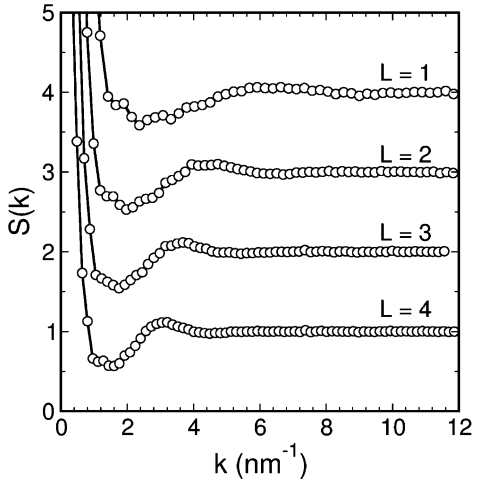

Figure 3. Structure factor $S(k)$ calculated as the Fourier transform of the NBB pair-correlation function. Successive curves are shifted by a factor of unity on the vertical axis for clarity.

Table 1. Model Network Properties

[a]L	1	2	3	4
[b]$t_{\text{cure}} \times 10^{-6}$	7.2	3.5	2.0	2.0
[c]unreacted linkers	0.10	0.14	0.19	0.23
[d]NBBs in network	0.995	0.999	0.998	0.997
[e]elastic material	0.93	0.88	0.84	0.79

[a] Number of segments per linker. [b] Time (in MC steps) for cross-linking. [c] Fraction of unreacted linkers in network. [d] Fraction of NBBs in network. [e] Fraction of network containing elastic material.

decreases with increasing L. The increase in network defects as L increases is expected because of the increased degree of steric hindrance introduced by the longer functional groups. Table 1 summarizes the cure times, the fraction of unreacted linker ends, the fraction of NBBs contained in the largest aggregate, and the fraction of elastic material in the network for each linker length.

We can better characterize the "completeness" of the network structure by looking at the number of linkers per NBB that have cross-linked to form tethers in the network. Figure 4 shows the time evolution (in Monte Carlo steps) of reacted linkers in the networks with linker lengths $L = 1$, 2, 3, and 4. The curves show the fraction of NBBs with 5, 6, 7, or 8 linkers reacted. At $L = 1$, the majority (~80%) of the tethered NBBs have at least seven linkers participating in the network, but at $L = 4$, only 40% of the NBBs have at least seven linkers in the network.

To test our model, we compare our predictions to experimental results for organic/inorganic networks made by cross-linking octafunctionalized POSS in solution.[13,46−49] We choose refs 13 and 26 for comparison because they offer the most complete characterization of these networks; a brief synopsis of their results follows. Octavinylsilsesquioxane, $[CH_2{=}CHSiO_{1.5}]_8$, was reacted with octahydridosilsesquioxane, $[HSiO_{1.5}]_8$, to form a network of cubic silsesquioxanes connected at the corners by tethers with two-atom backbones. The concentration of functionalized POSS in this system was 0.04 g/mL. Additional networks were made by reacting octa(vinyldimethylsiloxyl)silsesquioxane, $[CH_2{=}CHSi(CH_3)_2OSiO_{1.5}]_8$, with octahydridosilsesquioxane, $[HSiO_{1.5}]_8$, and octa(hydridodimethylsiloxyl)silsesquioxane, $[HSi(CH_3)_2OSiO_{1.5}]_8$, with octavinylsilsesquioxane, $[CH_2{=}CHSiO_{1.5}]_8$, to form cubic silsesquioxane networks connected by tethers with four-atom backbones and by reacting octa(hydridodimethylsiloxyl)silsesquioxane, $[HSi(CH_3)_2OSiO_{1.5}]_8$, with octa(vinyldimethylsiloxyl)silsesquioxane, $[CH_2{=}CHSi(CH_3)_2OSiO_{1.5}]_8$, to form cubic silsesquioxane networks connected by tethers with six-atom backbones. Characterization of the networks with nitrogen sorption, positron annihilation lifetime spectroscopy (PALS), and small-angle X-ray scattering (SAXS) revealed that the specific surface area and pore volume decreased as the length of the linkers increased. The network composed of two-atom tethers had a broad distribution of pore diameters (10−200 Å)[26] whereas the network with six-atom tethers had a narrow distribution of pore diameters (10−40 Å).[13] Wide-angle X-ray scattering (WAXS) curves[26] exhibited low-angle scattering peaks corresponding to correlation lengths of 8 Å for the network with two-atom tethers and 13 Å for the network with six-atom tethers. Solid-state NMR analysis showed that the degree of cross-linking increased as the length of the tethers increased, with the extents of reaction being 45% (two-atom tether), 66% (four-atom tether), and 81% (six-atom tether).

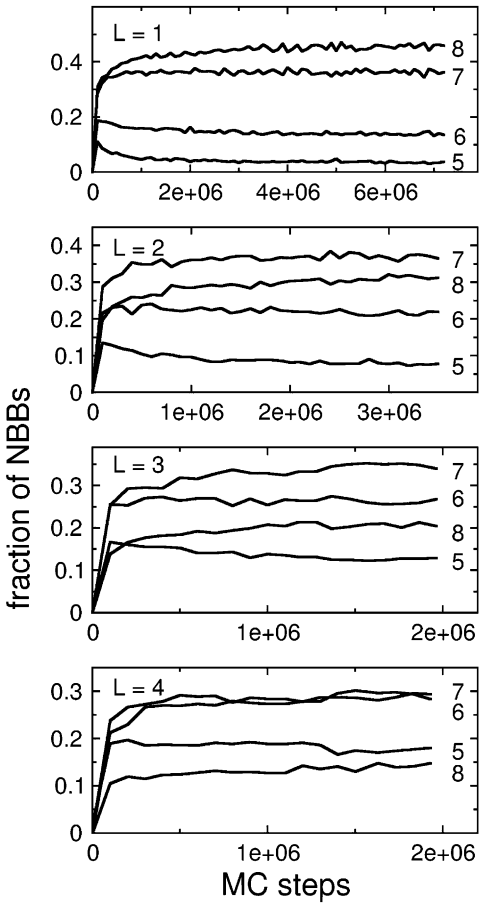

Figure 4. Extent of cross-linking in networks with (top to bottom) L equal to 1, 2, 3, and 4. The vertical axis indicates the fraction of NBBs in the system with a certain number of linkers that have cross-linked with linkers on other NBBs to form tethers. The numbers 5, 6, 7, and 8 labeling each curve specify the number of linkers that have cross-linked.

We now compare our model predictions with the experimental results for organic/inorganic hybrid networks of tethered POSS described above. Recall that in mapping our coarse-grained model to alkyl-POSS the $L = 1$ linker corresponds to approximately three backbone atoms so that the shortest model tether considered here is analogous to the longest tether studied in the above experiments. With regard to structure, the model predicts that porosity decreases as tether length increases, in agreement with the experimental results. The $S(k)$ results for the model network agree qualitatively with the WAXS data showing that the average spacing between the silsesquioxane cubes increases with increasing tether length. For the case of $L = 1$ (six-atom tether), we find an average spacing of 11 Å between silsesquioxane cubes, which differs slightly from the spacing of 13 Å indicated by the WAXS data in ref 26. With respect to the degree of cross-linking in the network, in the real system, the extent of reaction increases as tether length increases from two to six, but we find in the model system that the extent of reaction decreases as tether length increases beyond six. Combining the experimental results with our findings suggests that the six-atom tether may be the optimum length for balancing the competition between steric hindrance (due to the bulkiness of the functionalized silsesquioxane) and tether flexibility. For the case of the six-atom tether, the model predicts the extent of reaction to be 90% (i.e., seven or eight corners linked per cube), which slightly overestimates the experimental extent of reaction of 81% (i.e., six or seven corners linked per cube). This may be due to the fact that the model linker is more flexible than its experimental counterpart or because attractive interactions (other than cross-linking interactions) that may be present in the experimental system are neglected in the present study.

The simulations presented here required the use of a simplified model to access the long length and time scales needed to model the assembly process. Our minimal model captures the essential elements of connectivity and interaction specificity capable of predicting structures for a broad class of systems. In particular, because we have neglected interactions between NBBs in the present study, our model is immediately applicable to the assembly of nanoparticles whose interactions are screened, such as the case when oligonucleotides are grafted to the surface of gold nanoparticles,[20] and to the assembly of POSS building blocks when intercube interactions are effectively screened by the tethers. Experiments have shown that in cross-linked POSS networks composed of much longer (>110-atom backbone) tethers[26] and in polymers where POSS cubes are attached along the backbone as pendants[50,51] the POSS cubes have a tendency to phase segregate, suggesting the presence of attractive interactions between the silsesquioxane cubes. Increased chemical specificity can be included in the model through the addition of, for example, Coulomb or van der Waals interactions between groups of NBBs, between linkers, and between NBBs and linkers and the addition of, for example, directional or recognitive linking elements. Ab initio calculations of reaction mechanisms, for example, would be useful in estimating reaction rates that could be included for the latter; such computations are underway. Recent experiments[52] have shown that tuning the rigidity of the tether in POSS networks can have a remarkable impact on thermal and mechanical properties such as the glass-transition temperature and fracture toughness. Although the tethers considered here are relatively flexible, the rigidity of the organic tether could easily be adjusted in this model by introducing bond-angle potentials[53] along the tether backbone.

One limitation of the present model is that the functionalized building blocks reside on discrete lattice sites without the possibility of rotational motion. Nevertheless, our results indicate that even this crude model can capture key features of nanoscale assembly. Additional simulations on organic/inorganic nanostructured networks using this lattice model as well as off-lattice Monte Carlo, molecular dynamics, and Brownian dynamics simulation methods and combinations thereof to allow efficient access to multiple length and time scales are currently underway. Future modeling studies on assembled POSS/polymer networks will involve refining the coarse-grained model, introducing tether rigidity, and increasing the system size to probe the long length scale structural periodicity that appears to persist in these networks.

Acknowledgment. We thank J. Kieffer, R. M. Laine, P. T. Cummings, M. N. Neurock, C. McCabe, E. K. Lin, C. L. Soles, J. D. Lichtenhan, and M. J. Solomon for helpful discussions. Financial support for this work has been provided by the National Science Foundation under grant nos. DMR-0103399 and CTS-0210551. We thank the National Partnership for Advanced Computational Infrastructure (NPACI) and the University of Michigan Center for Advanced Computing for a generous allocation of CPU time on the AMD-Athlon cluster.

References

(1) Huynh, W. U.; Dittmer, J. J.; Alivisatos, A. P. *Science (Washington, D.C.)* **2002**, *295*, 2425−2427.
(2) Cassell, A. M.; Asplund, C. L.; Tour, J. M. *Angew. Chem., Int. Ed.* **1999**, *38*, 2403−2405.
(3) Sun, Y. G.; Xia, Y. N. *Science (Washington, D.C.)* **2002**, *298*, 2176−2179.
(4) Jin, R. C.; Cao, Y. W.; Mirkin, C. A.; Kelly, K. L.; Schatz, G. C.; Zheng, J. G. *Science (Washington, D.C.)* **2001**, *294*, 1901−1903.
(5) Pastoriza-Santos, I.; Liz-Marzan, L. M. *Nano Lett.* **2002**, *2*, 903−905.
(6) Sano, M.; Kamino, A.; Okamura, J.; Shinkai, S. *Nano Lett.* **2002**, *2*, 531−533.
(7) Chen, R. J.; Zhang, Y.; Wang, D.; Dai, H. *J. Am. Chem. Soc.* **2001**, *123*, 3838−3839.
(8) Qian, W. Y.; Rubin, Y. *Angew. Chem., Int. Ed.* **1999**, *38*, 2356−2360.
(9) Scott, L. T.; Boorum, M. M.; McMahon, B. J.; Hagen, S.; Mack, J.; Blank, J.; Wegner, H.; de Meijere, A. *Science (Washington, D.C.)* **2002**, *295*, 1500−1503.
(10) Shi, Z. Q.; Jin, J.; Li, Y. L.; Guo, Z. X.; Wang, S.; Jiang, L.; Zhu, D. B. *New J. Chem.* **2001**, *25*, 670−672.
(11) Laine, R. M.; Zhang, C. X.; Sellinger, A.; Viculis, L. *Appl. Organomet. Chem.* **1998**, *12*, 715−723.
(12) Feher, F. J.; Wyndham, K. D. *Chem. Commun.* **1998**, 323−324.
(13) Zhang, C. X.; Babonneau, F.; Bonhomme, C.; Laine, R. M.; Soles, C. L.; Hristov, H. A.; Yee, A. F. *J. Am. Chem. Soc.* **1998**, *120*, 8380−8391.
(14) Shockey, E. G.; Bolf, A. G.; Jones, P. F.; Schwab, J. J.; Chaffee, K. P.; Haddad, T. S.; Lichtenhan, J. D. *Appl. Organomet. Chem.* **1999**, *13*, 311−327.

(15) Choi, J.; Harcup, J.; Yee, A. F.; Zhu, Q.; Laine, R. M. *J. Am. Chem. Soc.* **2001**, *123*, 11420−11430.
(16) Costa, R. O. R.; Vasconcelos, W. L.; Tamaki, R.; Laine, R. M. *Macromolecules* **2001**, *34*, 5398−5407.
(17) Kim, B.-S.; Mather, P. T. *Macromolecules* **2002**, *35*, 8378−8384.
(18) Mitchell, G. P.; Mirkin, C. A.; Letsinger, R. L. *J. Am. Chem. Soc.* **1999**, *121*, 8122−8123.
(19) Qi, L. M.; Colfen, H.; Antonietti, M. *Nano Lett.* **2001**, *1*, 61−65.
(20) Mirkin, C. A.; Letsinger, R. L.; Mucic, R. C.; Storhoff, J. J. *Nature (London)* **1996**, *382*, 607−609.
(21) Alivisatos, A. P.; Johnsson, K. P.; Peng, X. G.; Wilson, T. E.; Loweth, C. J.; Bruchez, M. P.; Schultz, P. G. *Nature (London)* **1996**, *382*, 609−611.
(22) Niemeyer, C. M.; Burger, W.; Peplies, J. *Angew. Chem., Int. Ed.* **1998**, *37*, 2265−2268.
(23) Korgel, B. A.; Fullam, S.; Connolly, S.; Fitzmaurice, D. *J. Phys. Chem. B* **1998**, *102*, 8379−8388.
(24) Mann, S.; Shenton, W.; Li, M.; Connolly, S.; Fitzmaurice, D. *Adv. Mater.* **2000**, *12*, 147−150.
(25) Boal, A. K.; Ilhan, F.; DeRouchey, J. E.; Thurn-Albrecht, T.; Russell, T. P.; Rotello, V. M. *Nature (London)* **2000**, *404*, 746−748.
(26) Soles, C. L.; Lin, E. K.; Wu, W. L.; Zhang, C.; Laine, R. M. *Organic/Inorganic Hybrid Materials*; Materials Research Society: Warrendale, PA, 2000; Vol. 628.
(27) Carmesin, I.; Kremer, K. *Macromolecules* **1988**, *21*, 2819−2823.
(28) Deutsch, H. P.; Binder, K. *J. Chem. Phys.* **1991**, *94*, 2294−2304.
(29) Paul, W.; Binder, K.; Heermann, D. W.; Kremer, K. *J. Chem. Phys.* **1991**, *95*, 7726−7740.
(30) Hagn, C.; Wittkop, M.; Kreitmeier, S.; Trautenberg, H. L.; Holzl, T.; Goritz, D. *Polym. Gels Networks* **1997**, *5*, 327−337.
(31) Gilra, N.; Cohen, C.; Panagiotopoulos, A. Z. *J. Chem. Phys.* **2000**, *112*, 6910−6916.
(32) Trautenberg, H. L.; Sommer, J. U.; Goritz, D. *J. Chem. Soc., Faraday Trans.* **1995**, *91*, 2649−2653.
(33) Schulz, M.; Sommer, J. U. *J. Chem. Phys.* **1992**, *96*, 7102−7107.
(34) Chen, Z.; Cohen, C.; Escobedo, F. A. *Macromolecules* **2002**, *35*, 3296−3305.
(35) Michalke, W.; Kreitmeier, S.; Lang, M.; Buchner, A.; Goritz, D. *Comput. Theor. Polym. Sci.* **2001**, *11*, 459−466.
(36) Michalke, W.; Lang, M.; Kreitmeier, S.; Goritz, D. *J. Chem. Phys.* **2002**, *117*, 6300−6307.
(37) Schulz, M.; Frisch, H. L. *J. Chem. Phys.* **1994**, *101*, 10008−10022.
(38) Di Cecca, A.; Freire, J. *Macromolecules* **2002**, *35*, 2851−2858.
(39) Bieniok, A. M.; Burgi, H. B. *J. Phys. Chem.* **1994**, *98*, 10735−10741.
(40) Bartsch, M.; Bornhauser, P.; Calzaferri, G.; Imhof, R. *J. Phys. Chem.* **1994**, *98*, 2817−2831.
(41) Several sophisticated schemes for mapping coarse-grained polymer models to their atomistic counterparts have been reviewed recently. See, for example, Baschnagel, J.; Binder, K.; Doruker, P.; Gusev, A. A.; Hahn, O.; Kremer, K.; Mattice, W. L.; Muller-Plathe, F.; Murat, M.; Paul, W.; Santos S.; Suter, U. W.; Tries, V. *Adv. Polym. Sci.* **2000**, *152*, 41.
(42) Atomistic models of octa(propyl)-, octa(butyl)-, octa(pentyl)-, and octa(hexyl)-POSS were built and minimized in Cerius2 using a combination of the steepest descent and truncated minimization algorithms. The interactions between atoms were given by the COMPASS force field.
(43) Paul, W.; Binder, K.; Heermann, D. W.; Kremer, K. *J. Phys. II* **1991**, *1*, 37−60.
(44) Chen, T.; Lamm, M. H.; Glotzer, S. C. To be submitted for publication.
(45) Nijenhuis, A.; Wilf, H. S. *Combinatorial Algorithms*; Academic Press: New York, 1975.
(46) Hoebbel, D.; Pitsch, I.; Heidemann, D. In *EUROGEL '91*; Vilminot, S., Nass, R., Schmidt, H., Eds.; North-Holland: Amsterdam, 1992.
(47) Hoebbel, D.; Endres, K.; Reinert, T.; Pitsch, I. *J. Non-Cryst. Solids* **1994**, *176*, 179−188.
(48) Harrison, P. G.; Kannengiesser, R. *Chem. Commun.* **1996**, 415−416.
(49) Morrison, J. J.; Love, C. J.; Manson, B. W.; Shannon, I. J.; Morris, R. E. *J. Mater. Chem.* **2002**, *12*, 3208−3212.
(50) Mather, P. T.; Jeon, H. G.; Romo-Uribe, A.; Haddad, T. S.; Lichtenhan, J. D. *Macromolecules* **1999**, *32*, 1194−1203.
(51) Jeon, H. G.; Mather, P. T.; Haddad, T. S. *Polym. Int.* **2000**, *49*, 453−457.
(52) Choi, J.; Yee, A. F.; Laine, R. M., submitted for publication.
(53) Tries, V.; Paul, W.; Baschnagel, J.; Binder, K. *J. Chem. Phys.* **1997**, *106*, 738−748.

NL034090S